

Deep Excavation Analysis Supported by Anchored Diaphragm Walls: A comparison of Constitutive Models

Hind K. Nasir¹ and Rafi' M. Sulaiman Al-Ne'aimi²

^{1,2} Department of Civil Engineering / College of Engineering / University of Duhok / 1006 AJ Duhok, KR-Iraq

ABSTRACT: This paper presents a numerical study of a large and deep excavation in clay soil supported by anchored diaphragm walls under unequal load to investigate the influence of several design parameters on the stability and safety of the supporting system and their impacts on the surrounding nearby structures using the Plaxis 2D v20 code. The numerical model result was compared with a case study of braced excavation in the clays, and a close match between the results was observed. The soil profile consists of several clay layers and is modeled with two constitutive modes: the Mohr-Coulomb model (MCM) and the hardening soil with a small strain model (HSsmall). The diaphragm walls were modeled as plates and the anchor rods as node-to-node connections. The studied parameters include the inclination angle of anchors, number of ground anchors, surface load magnitude, various ratios of wall-embedded depth to the excavation depth on a deep excavation, and the heave developed at the bottom of the excavation. It was observed that as D_e / D_{ex} is increased from 0.3 to 0.5, u^{xw} and M is reduced by approximately 6.7% and 14.7%, respectively, for the MCM, compared to 10.5% and 8.1% by the HSsmall modeling. Whereas D_e / D_{ex} increased to 0.7, the values of u^{xw} and M in both models remained unchanged. Furthermore, for all studied D_e / D_{ex} ratios, the MCM produces around 28 mm of heave compared to 23 mm for the HSsmall model. In general, the outcome results of the analysis were examined and discussed in terms of maximum values of lateral displacements, bending moments in the wall supporting system, and the settlement of the ground surface behind both sides of the excavation, which can serve as a reference for deep excavation design and similar geotechnical problems.

Keywords: Constitutive models; Deep excavation; Diaphragm walls; Embedded depth; Heave; Numerical analysis.

1. Introduction

Deep excavations always result in lateral and vertical ground deformations. The majority of the vertical deformations are downward deformations (settlements) or upward deformations (heaves) observed close to or far from the wall supporting system. According to El-Nahhas and Morsy (2002), and Fayed (2002), the techniques for obtaining deep excavation deformations can be categorized as empirical and semi-empirical methods; numerical and analytical methods; physical and centrifuge modeling, and an artificial neural network approach (ANNs). The assessment of deformations caused by deep excavation is also affected by whether or not a building is nearby.

Geotechnical engineers often face difficulties in choosing the reliable soil model to be utilized for the numerical analysis and gives a reasonable fit to data obtained from a variety of laboratory tests. Schweiger and Breymann (2006) used the Hardening Soil (HS) model in PLAXIS finite element software for the analysis of five distinct deep excavations in soft clay and the comparison of results with in-situ measurements. They concluded that the HS model gives more accurate results when modeling such problems. Schweiger (2007) used the elastic-plastic soil behavior constitutive model to evaluate its impact on calculated displacements and bending moments in a diaphragm wall of deep excavation. The parameters involved include wall friction, the domain chosen for the analysis, constitutive models, and grout body modeling. The results proved that the constitutive model used could not capture the realistic deformations for these kinds of issues. Based on a comparison of three soil models with real measurements Schweiger (2009) concluded that for FE analyses, a more advanced constitutive model is necessary to obtain reliable results

compared to the MCM. These findings were confirmed by Zain et al. (2011), who found that the results of the MC model were nearly close to those of the HS model in terms of horizontal displacements in clay due to excavation; however, the difference in soil stresses is high resulting from the different characteristics of the two models, especially that the HS model uses three different stiffness parameters, which are E_{50} , E_{ur} , and E_{oed} , while the MC model only considers Hooke's single stiffness with linear elasticity. Similarly, Capraru and Chirica (2012) stated that the hardening soil model gives a better correlation between measured and calculated deflections of the wall than the Mohr-Coulomb model. This is due to the two models' different descriptions of nonlinear soil behavior (e.g., soil stiffness in different strain ranges).

Due to the complex nature of soil-support system interactions (diaphragm walls are usually used) induced by the nonlinear behavior of the soil, fluctuations in the groundwater level, and the staged phasing of the excavation and the installation of ground anchors, numerical simulations are widely used in the design and analysis of deep excavations. As a case study, Chowdhury et al. (2013) used the PLAXIS FE code for the analysis of the excavation of the Sukhumvit Station of the Bangkok MRT underground construction project. Higher levels of constitutive models, namely SSM, HSM, and HSsmall, were used to provide improved lateral wall motions and ground surface settlements. However, there are no salient differences between the estimates for axial force, shear force, and bending moment. Kulkarni (2014) presented a study of the deep basement excavation of a thirty-three-story high-rise tower using the FE software PLAXIS 2D. Contiguous bored piles are used as a retaining wall supporting system that is anchored at three levels for evaluation of the bending moment in the wall and settlement of the ground. The results indicate that the moment on the wall increases as the excavation depth increases. Johansson and Sandeman (2014) showed that in the absence of triaxial tests, basing an MCM on empirical correlations to evaluate the stiffness can give fairly accurate results. While it is not so in the case of HSsmall because there are different methods of correlating these parameters that give different results. Tjie-Liong (2014) outlined some errors when using Plaxis 2D software to analyze excavation issues. These are: failure in selecting the appropriate model for plane strain versus axisymmetry; applying the interface element when modeling pressure grouted ground anchors is a common mistake; when the MC model is used, it is advised to input the soil stiffness in E_{ur} value rather than E_{50} , but when the Hardening model (HS) is used, each of the loading stiffness, E_{50} , the unloading-reloading modulus, E_{ur} , and the oedometer modulus, E_{oed} , should be taken into account."

Korff et al. (2012), and Mitew-Czajewska (2017) noted that most of the elastic-perfectly plastic Mohr-Coulomb constitutive models have several limitations, and as a result, they give excessive settlements of the surrounding soil, which is not observed in practice. Mitew-Czajewska (2018) showed that for deep excavation in clays, the use of the Hypoplastic Clay model produced very good mapping (only up to a 13% difference compared to the real displacement), whereas the HS or HSsmall models produced no heave of the ground surface in the influence zone behind the wall, and the settlement values directly behind the excavation walls were significantly overestimated (being up to 7.5 times higher than measured settlement values). Abdel-Fattah et al. (2018) investigated the effects of varying the inclination of ties in the sand, wall height, and groundwater level on the behavior of anchored sheet pile walls. It was found that an increase in the inclination angle of the ties up to 20° decreases each of the maximum bending moments and maximum lateral deflections of the wall, whereas the anchor forces slightly increase. By increasing the inclination angle more, all of the maximum bending moments, horizontal displacements of the wall, and anchor forces increase."

Engin (2019) used PLAXIS 2D with three different constitutive soil models to perform a back analysis on a 25-meter-deep excavation supported by contiguous bored piles and a multilayered anchorage system in Ankara clay. The study aimed to evaluate the performance of these material models concerning their capability of estimating the measured displacement distribution along the depth and to compare the models with each other and with inclinometer measurement data along the depth of excavation. It is observed that the displacements obtained from the HSsmall model results are closest to the real displacements than the MC model, and the load-settlement relations obtained from the HS and HSsmall models are very close to each other. Similar displacement back analyses were

conducted by Li et al. (2019), who found that the difference in results of the MC model and the HSsmall model increases with the increase of excavation depth. It is reported that when the excavation depth exceeds 15 m, the HSsmall model should be used since its results are more realistic to the actual deformation. Based on the monitoring data of the deep foundation pits of 15 subway stations in Shanghai and Ningbo cities around Hangzhou, Mei et al. (2021) clarified the deformation law during the excavation of a deep foundation pit in a soft soil region. The results provide a guideline reference for the targeted design and construction of the diaphragm wall of a deep-foundation pit. The results also noted that the maximum lateral deformation of the wall increases linearly with the relative depth of the maximum lateral deformation.

This paper presents a numerical analysis to study the influence of several design parameters on the stability of anchored diaphragm walls of large and deep excavation in clay soil and their effects on safety against nearby structures in terms of lateral displacement, bending moments in the wall supporting system, the settlement of the ground surface in the influence zone, and the heave at the bottom of the excavation.”

2. Method of analysis

2.1 Model Geometry Boundaries and Mesh Generation

The soil profile used in this study is related to a proposed 45-floor multi-story high-rise building in Duhok City, in the Kurdistan Region of Iraq. It consists of four layers of different properties with an overall depth of 45 m based on the site investigation report and average properties of logs of borings. The groundwater table (G.W.T.) is encountered at 16 m below the ground surface. The created numerical model consists of four material components: (1) soil elements; (2) plate elements for modeling the diaphragm wall supporting systems; (3) embedded beam rows for modeling anchor grout bodies; and (4) node-to-node for simulating anchor rods. The model boundaries are selected with the bottom boundary as fully rigid, whereas the edge boundaries are rigid in the two horizontal directions only. After the soil and structural models, loads, and boundaries are completely defined, a fully automatic mesh generation is performed. For accurate results, the global coarseness is set to “fine” mesh refinement with a relative element size of 0.333. As a case example, Figure 1 shows a typical finite element model geometry and meshing consisting of 6699 elements and 54757 nodes.

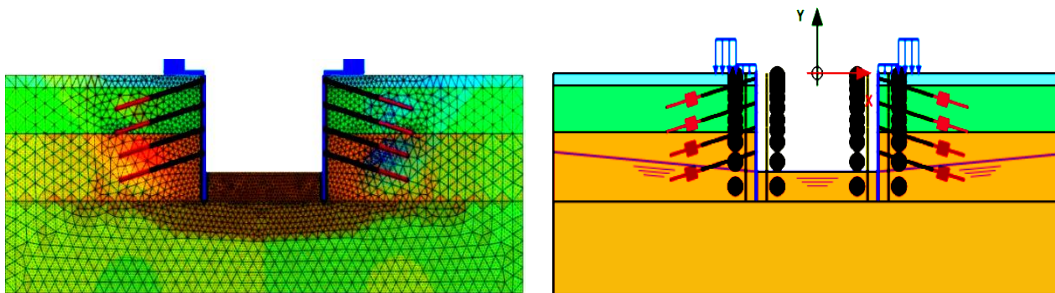


Figure 1: Finite element model geometry and meshing.

2.2 Finite Element Software and Constitutive Models Used

In this study, the PLAXIS 2D v20 software was used for numerical modeling and analysis. This software is a professional finite element package developed specifically for the analysis of deformation and stability problems in geotechnical engineering, including static or dynamic nonlinear finite element analysis of various geotechnical problems. Two constitutive models are used for modeling the soil layers. These are:”

2.2.1 Mohr-Coulomb's Model (MCM)

This model is an elastic-perfectly plastic model, and its behavior is illustrated in Figure 2a. Five input parameters are required for the model: E and ν for the elasticity, ϕ and c for plasticity, and φ for the dilatancy. The model is isotropic and does not account for soil stress dependence, i.e., soils' tendency to stiffen with increased pressure. Plaxis recommends using this material model in an initial simulation of soil because it is relatively fast and fairly accurate. The yield condition in this model consists of six yield functions. When these functions are set to zero (i.e., acting plastic), they create a surface in the principal stress space called the yield surface. Within it any material acts as elastic, and Hooke's law obeys. See Figure 2b.

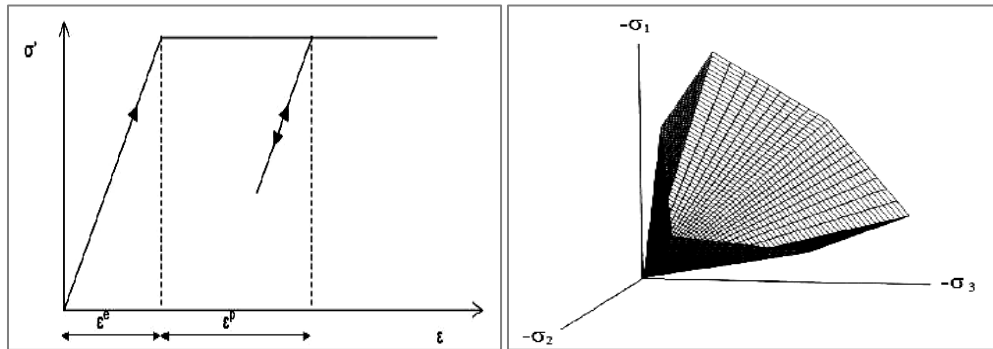


Figure 2: (a) Basic idea of an elastic perfectly plastic model, (b) Yield surface in principle stress space (Plaxis 2020, Manual).

2.2.2 Hardening Soil Model with Small Strain (HSsmall)

It is an advanced model that has a cap yield surface and can more accurately reproduce soil deformations than the simple elastic-perfect plastic, the "Mohr-Coulomb" model Obrzud (2010). As well as, in this model, the stress-strain-relation is non-linear and the soil stiffness is calculated using three different stiffnesses (triaxial loading secant stiffness, triaxial unloading/reloading stiffness, and oedometer loading tangent stiffness). See Figure 3."

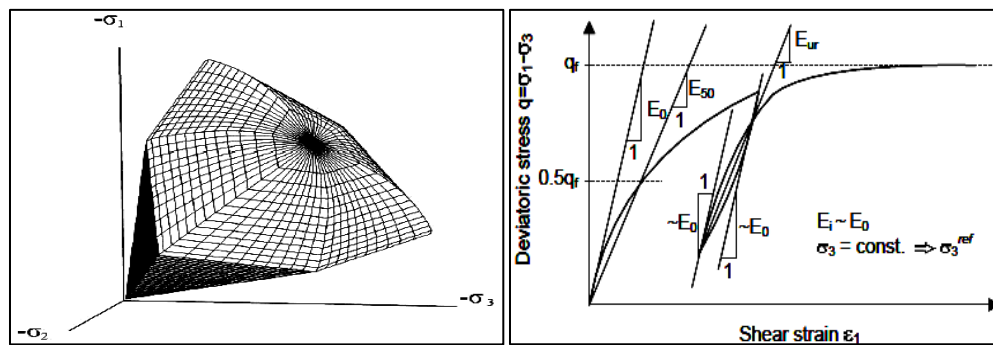


Figure 3: (a) Different moduli of typical stress-strain curve of soil, (b) The cap yield surface in principle stress space (Plaxis 2020, Manual)

In both models, the soil elements are modeled using 15-noded triangular elements with two translational degrees of freedom per node that contain 12 stress points. The plates used for modeling diaphragm walls are modeled as beam elements of 5 nodes with three degrees of freedom per node: two translational degrees of freedom u_x, u_y and one rotational degree of freedom, each beam element is defined by five nodes that contain four pairs of Gaussian stress points. Within each pair, stress points are located at a distance $1/6\sqrt{3}d_{eq}$ above and below the plate centerline. The formulations of plating elements are based on Mindlin's plate theory Bathe (1996). The soil and the structural

elements are schematically shown in Figure 4. The soil parameters for each layer are shown in Table 1, whereas the properties for the diaphragm walls as plates, anchor rods as nod-to-node, and grout body as embedded beam rows are presented in Tables 2-4.

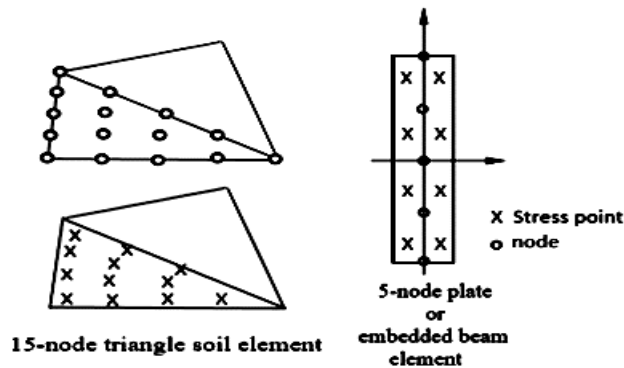


Figure 4: Types of elements, position of nodes and stress points used in analysis (Brinkgreve et al. 2019)

Table 1: Parameters for (MCM) and (HSsmall) models' analysis Likitlersuang et al. (2013).

Parameter	Soil type layers			
	Backfill soil	Soft clay	Stiff clay	Hard clay
Thickness (m)	0–2.5	2.5–12	12–26	26–45
Material model	HS small	HS small	HS small	HS small
Analysis type	Drained	Undrained	Undrained	Undrained
Unit weight, γ_{unsat} (kN/m ³)	18	16.5	20	20
Saturated unit weight, γ_{sat} (kN/m ³)	20	19	20	20
Initial void ratio, e_o	0.5	0.5	0.5	0.5
Cohesion, c' (kPa)	10	40	50	80
Internal friction angle, ϕ^o	25	26	28	30
Dilatancy angle, ϕ^o	0	0	0	0
Secant stiffness from a drained triaxial test, E_{50}^{ref} (MPa)	45.6	0.8	8.5	30
Tangent stiffness for oedometer primary loading, E_{oed}^{ref} (MPa)	45.6	0.85	9.0	30
Unloading/reloading stiffness, E_{ur}^{ref} (MPa)	136.8	8.0	30	120
Unloading/reloading Poisson's ratio, ν_{ur}	0.2	0.2	0.2	0.2

Table 1: Continued.

Rate of stress dependency, m	1.0	1.0	1.0	1.0
Coefficient of earth pressure at rest, K_o^{nc}	0.58	0.56	0.53	0.5
Failure ratio, R_f	0.9	0.9	0.9	0.9
Shear strain amplitude at 0.722 G_{max} , $\gamma_{0.7}$	1.5×10^{-4}	1.2×10^{-4}	2.5×10^{-4}	2.5×10^{-4}

Ref. small strain shear modulus, G_0^{ref} (MPa)	100	60	12.5	200
Interface reduction factor, R_{inter}	0.8	0.8	0.8	0.8

Table 2: Properties of the diaphragm walls as a plate (assumed according to Schweiger (2007))

Parameter	Wall thickness, d (m)			
	0.6	0.8*	1.0	1.2
Type of behavior	Elastic Isotropic	Elastic Isotropic	Elastic Isotropic	Elastic Isotropic
Normal Stiffness, EA (kN/m)	18×10 ⁶	24×10 ⁶	30×10 ⁶	36×10 ⁶
Flexural rigidity, EI (kNm ² /m)	0.54×10 ⁶	1.28×10 ⁶	2.5×10 ⁶	4.32×10 ⁶
Weight, w (kN/m/m)	7.5	7.5	7.5	7.5
Poisson's ratio, ν	0.15	0.15	0.15	0.15

* (after Schweiger, 2007)

Table 3: Properties of the anchor rods as node-to-node assumed according to Mitew-Czajewska (2018)

Parameter	Value
Material Type	Elastic
Normal Stiffness, EA (kN/m)	Anchor 1 (3.0×10 ⁵)
	Anchor 2 (4.0×10 ⁵)
	Anchor 3 (6.0×10 ⁵)
	Anchor 4 (6.0×10 ⁵)
Spacing out-of-plane, L _s (m)	Anchor 1 & 2 (2.5)
	Anchor 3 & 4 (1.5)

Table 4: Properties of the grout body as embedded beam rows assumed according to Mitew-Czajewska (2018)

Parameter	Value	
	Rows 1 & 2	Rows 3 & 4
Material Type	Elastic	Elastic
Stiffness, E (kN/m ²)	3.0× 10 ⁶	7.0× 10 ⁶
Unit weight, γ (kN/m ³)	24	24
Beam type	Predefined	Predefined
Predefined beam type	Massive circular beam	Massive circular beam
Diameter, D (m)	0.2	0.3
Pile spacing, L _{spacing} (m)	2.5	1.5
Skin resistance	T _{skin,start,max} (kN/m)	400
	T _{skin,end,max} (kN/m)	400
Base resistance, F _{max} (kN)	400	600
Interface stiffness actor	Default values	Default values

2.3 Validation of the Finite Element Model

To ensure Plaxis' accuracy in analysis, the numerical model results were compared to those reported by Mitew-Czajewska (2018) for the case study of a 20-m wide, 14.6-m deep, and 150-m long excavation in three-layered soils at the Warsaw Metro Station with a supporting system consisting of two diaphragm walls with two layers of ground anchors and one level of steel struts. The typical cross-section, including nine construction phases and geotechnical

conditions, is shown in Figure 5. For further information on the soil layers and the structural element parameters, see Mitew-Czajewska (2018).

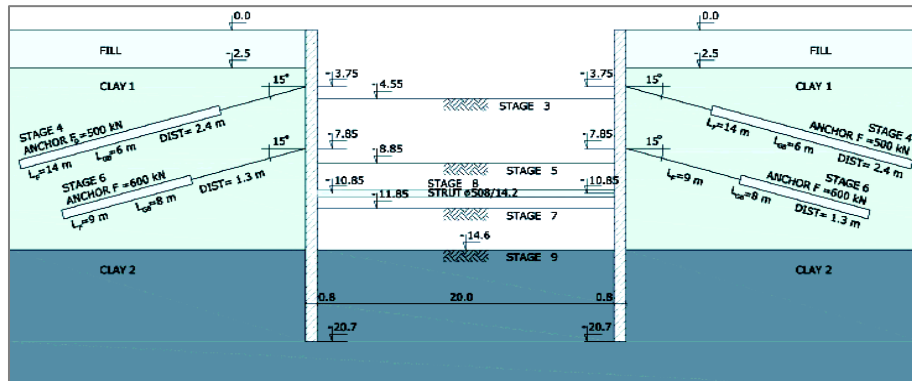


Figure 5: Typical cross-section, (after Mitew-Czajewska (2018)).

As illustrated in Figure 6, the comparison of analysis results showed a close match between the results in terms of both trend and magnitude. Furthermore, in Figure 6, the present model also matches the measured values more closely than those predicted numerically by Mitew-Czajewska (2018). Thus, now the verified model can be used for conducting the parametric study to investigate the influence of several design factors on the performance of an anchored diaphragm wall supporting system.

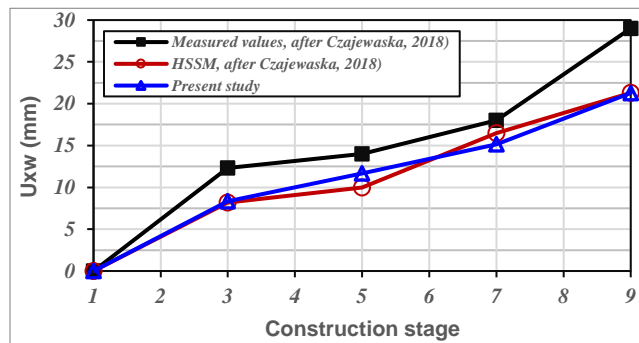


Figure 6: Horizontal displacements u_{xw} of the top of the wall versus construction stages.

3. Parametric study testing program schedule

The effects of several design parameters that significantly influence deep excavation are investigated through a numerical analysis carried out as a plane strain problem using the Plaxis 2D v20 code. The case example used for the analysis is an excavation width of $B = 30$ m, an excavation depth of $D_{ex} = 20$ m, and a round 70-meter-long excavation of a proposed 45-story high-rise building in Duhok City, Kurdistan Region, Iraq. The parameters studied include the inclination angle of anchors (α^o), the number of ground anchors, surface load magnitude, and the wall embedded depth to excavation depth ratio (D_b / D_{ex}) in layered soil. It also examines the impact of the excavation on the safety of the surrounding nearby structures through the detection of the lateral displacement at the top of the supporting system (u_{xw}); the bending moment developed in the supporting system (M); the vertical displacements of the ground surface (v) in the zone of influence; and the heave develop at the bottom of the excavation (u_y) which can serve as references for deep excavation design and similar geotechnical problems. Details of the testing program schedule with all the varying studied parameters are shown in Table 5.

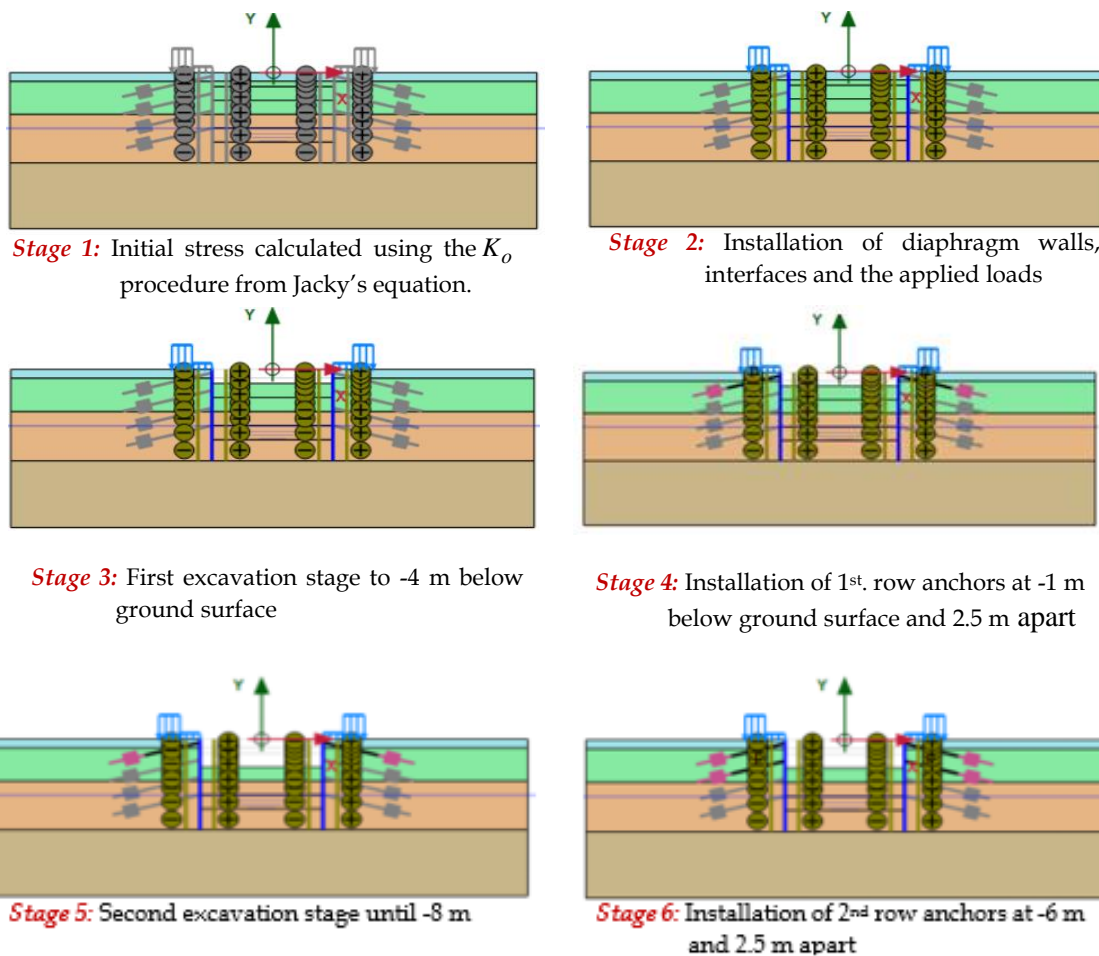
Table 5: Details of the testing program schedule.

Test No.	The inclination angle of anchors (α°)	No. of anchors	Surface load magnitude (kPa)	Wall-embedded excavation depth ratio (D_b/D_{ex})	Constitutive Models	Studied Parameter*
1-5	0,10,15,20,25	4	Left:10+40 Right: 20	0.3	HSsmall	Angle of anchor inclination
6-23	15	3,4,5	Left & right 10+40	0.3 0.5 0.7	HSsmall MC	Number of anchors
24-31	15	4	Left & right 0,20,30,40	0.3	HSsmall MC	Surface load magnitude
32-49	15	3,4,5	Left & right 10+40	0.3 0.5 0.7	HSsmall MC	Basal Heave

* For all tests: wall thickness = 0.8 m, and the GWT at 16 m below ground.

3.1 Stages of construction

The calculation process of the model consists of multiple phases defined due to the construction sequence and loading in the staged construction mode. The sequence of analyses for $D_p/D_{ex} = 0.3$ (i.e., a 26 m diaphragm wall with four ground anchors and groundwater at -8 m below the ground surface) is presented in Figure 7.



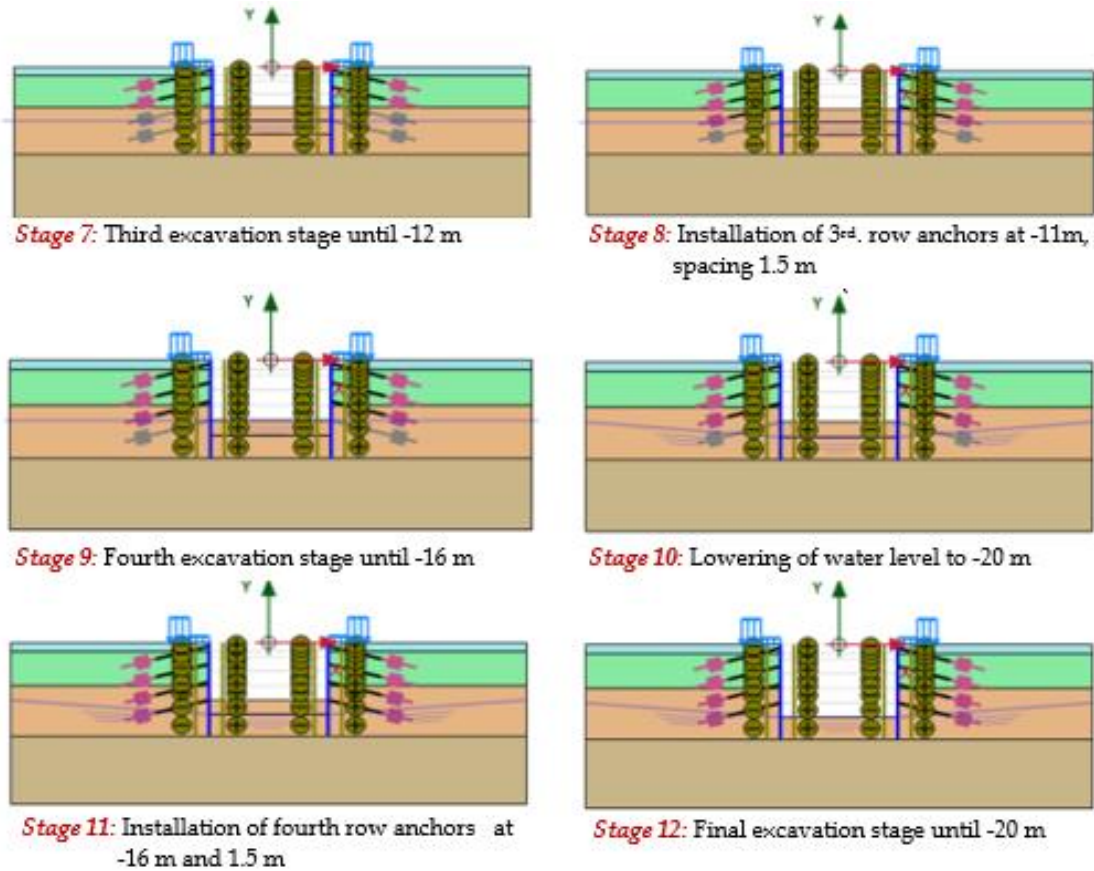


Figure 7: Construction stages for $D_p/D_{ex} = 0.3$ as example.

Once all stages are set up and defined, a nonlinear elastic-plastic deformation analysis is performed from stage 2 to the final one with an iterative procedure and automatic load stepping control is used for each stage.

4. Results and Discussions

4.1 Effect of Anchor Inclination Angle

Five different ground anchor angles (0° , 10° , 15° , 20° , and 25°) were considered to study the effect of the anchor inclination angle on 20 m excavation depth D_{ex} , and 30 m excavation width under certain conditions: wall embedded to excavation depth ratio $D_b/D_{ex} = 0.3$, two diaphragm walls each of $t_{wall} = 0.8$ m, the groundwater $D_w = 16$ m below the ground surface, the number of used anchors equal to 4, the load behind the left diaphragm wall is 10+40 kPa and that behind the right wall is 20 kPa. Both loads started at 0 m and are extended to 10 m from both excavation edges. The variations of the maximum u_{xw} and M in the diaphragm walls with α° at the end of the final excavation stage are shown in Figure 8 (a, and b). It can be seen that increasing the ground anchor angle α° up to 15° results in a decrease in maximum u_{xw} and M then their values increase slightly when α° increased from 15 to 25. A similar trend was observed in both diaphragm walls, although the surface-applied load behind each wall is different. The optimum values of u_{xw} and M were obtained at $\alpha = 15^\circ$ as demonstrated by their values in the left diaphragm wall of 59.20 mm, and 843.20 kN.m/m, respectively, and in the right diaphragm wall of 52.71 mm, and 875.4 kN.m/m, respectively. The influence of α° on the ground surface settlement at the end of the final excavation stage is shown in Figure 8 (d). This figure shows that the ground surface settlement on both sides

of the excavation similarly decreases with an increase in the anchor inclination angle up to $\alpha = 15^\circ$, then slightly increases. Therefore, the optimum result in the ground surface settlement is obtained when $\alpha = 15^\circ$. This result is observed on both sides of the excavation behind diaphragm walls. Figure 9 shows the variations of u_{xw} , M , and v in the LDW (as an example) with depth and α at the end of the final excavation stage.

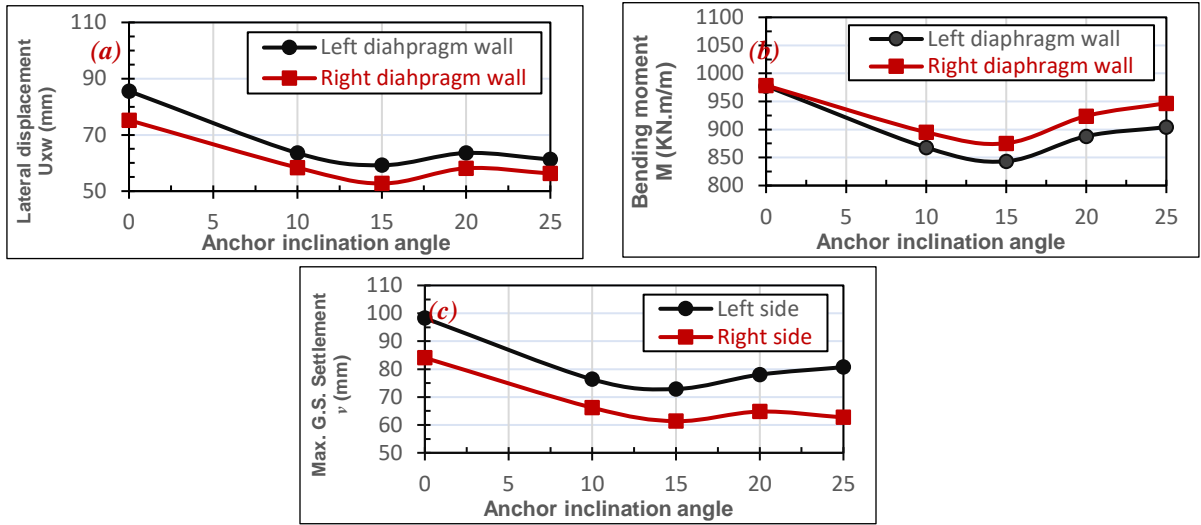


Figure 8: Variations of u_{xw} , M , v with α° for $(D_b/D_{ex} = 0.3)$ –final excavation.

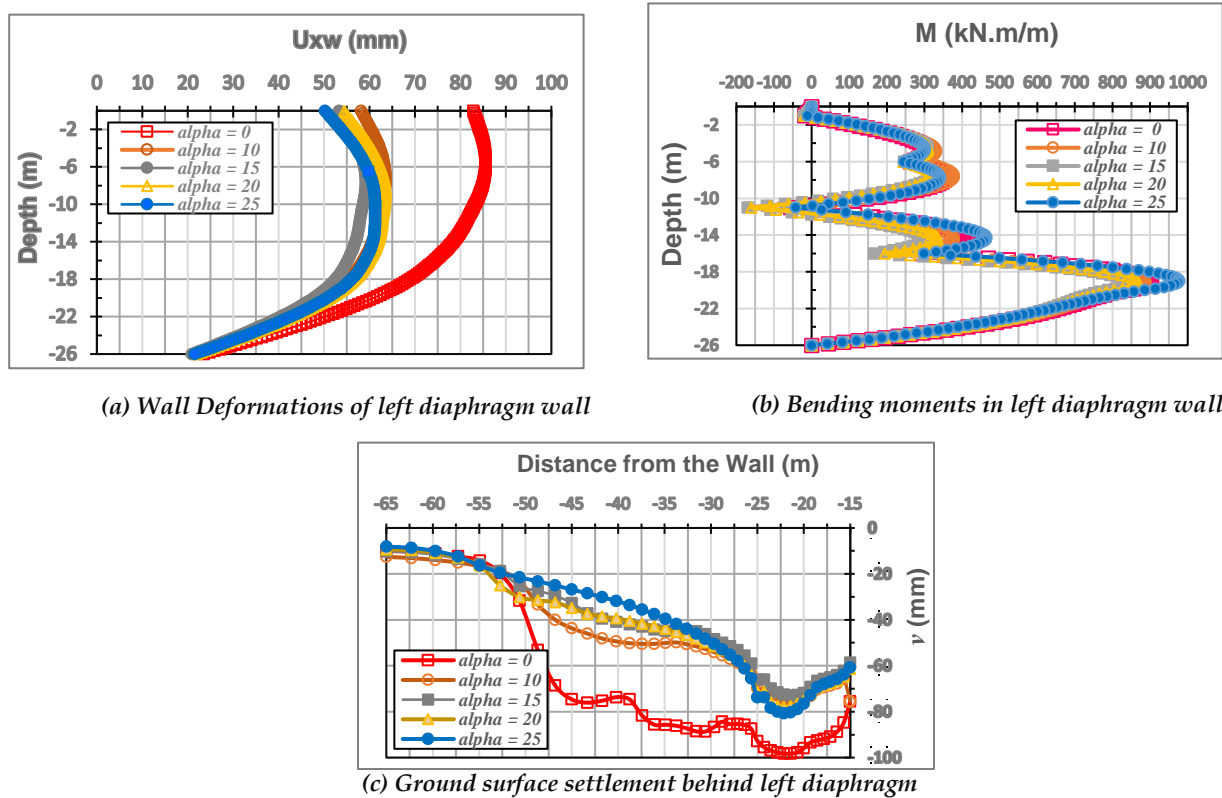


Figure 9: Variations in u_{xw} , M , and v with α° and depths for $(D_b/D_{ex} = 0.3)$ –final excavation.

The variation of maximum ground settlement (v) with α^o and for all excavation stages under the applied loads starting at 0 m from the edges of the excavation is presented in Table 6. As shown, the ground surface adjacent to the excavation settles more and more with the excavation's progress; however, this settlement is influenced by the presence of the load near the excavation area. In addition, analysis of different stages gives different values of the settlement for each particular stage, and the location of the maximum settlement varies from case to case.

Table 6: Variation of maximum ground surface settlement (v) with α^o for ($D_b / D_{ex} = 0.3$).

Construction Stage	Maximum ground surface settlement behind the left diaphragm wall (v) (mm)				
	$\alpha = 0^o$	$\alpha = 10^o$	$\alpha = 15^o$	$\alpha = 20^o$	$\alpha = 25^o$
1st. Excavation	32.18	32.15	32.21	32.66	32.72
2nd. Excavation	47.69	46.43	46	46.94	46.85
3rd. Excavation	58.59	54.74	53.57	55.61	55.15
4th. Excavation	75.22	63.08	60.44	63.34	62.79
Final Excavation	98.27	76.35	72.88	78.03	80.71

4.2 Effect of the Number of Ground Anchors

In this series, 3, 4, and 5 ground anchors at an inclination angle $\alpha = 15^o$ were used to study their effects on the maximum values of lateral wall displacements, and bending moments in the walls each of 0.8 m thickness for different D_b / D_{ex} ratios. The analysis was carried out for MC and HSsmall constitutive models, $D_w = -16$ m below the ground surface, and the applied loads of 10 + 40 kPa started from 0 m and extended to 10 m lengths from both excavation sides. The effect of the anchor numbers on maximum values of u_{xw} and v at the end of the final excavation stage is illustrated in Figure 10. It was observed that for both MC and HSsmall soil modeling, the variations of all outcome values decreased significantly with an increase in anchor number up to 4 and then after the rate of reduction was minimized.

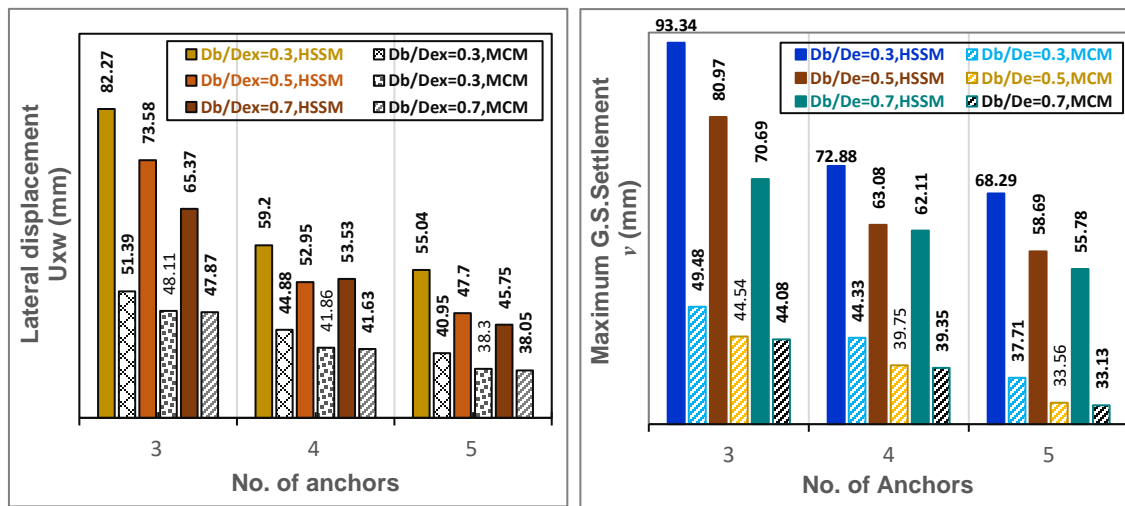
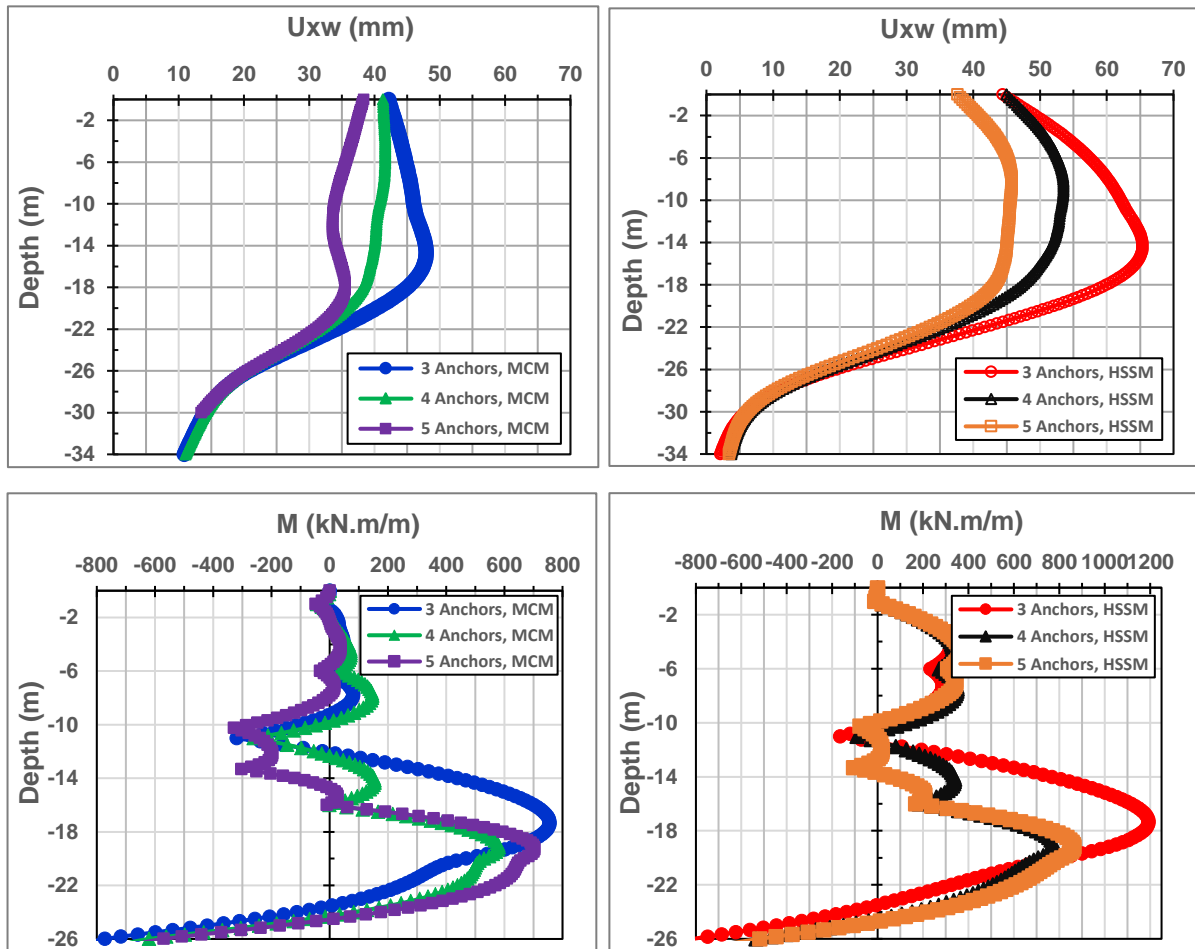


Figure 10: Variations in u_{xw} and v with number for anchors for all (D_b / D_{ex}).

As shown in Figure 10 when the number of anchors increased from three to four, the behavior of the supporting system significantly improved, since the values of u_{xw} in the wall for MC and HSsmall models decreased by 13%, and 28% respectively, and when increasing the number of anchors to five, these ratios decreased to 9% and 7%, for both models, respectively. A similar trend was observed for the maximum ground surface settlement v as their values significantly decrease to 10% and 22% for MC and HSsmall models when the number of anchors increased from three to four, after which little improvement was attained in the values of v ; Thus, based on these observations, four ground anchors will be used as supports for the walls on each side of the excavation for all the remaining analyses.

The variations of u_{xw} and M in the walls across their depths and the ground surface settlement v behind each excavation side with anchor numbers at the end of the final excavation stage for $D_b / D_{ex} = 0.7$ is illustrated in Figures 11 and 12, respectively.



(a) MC model

(b) HSS with small stain model

Figure 11: Variations in u_{xw} , and with anchor numbers for $(D_b / D_{ex} = 0.7)$.

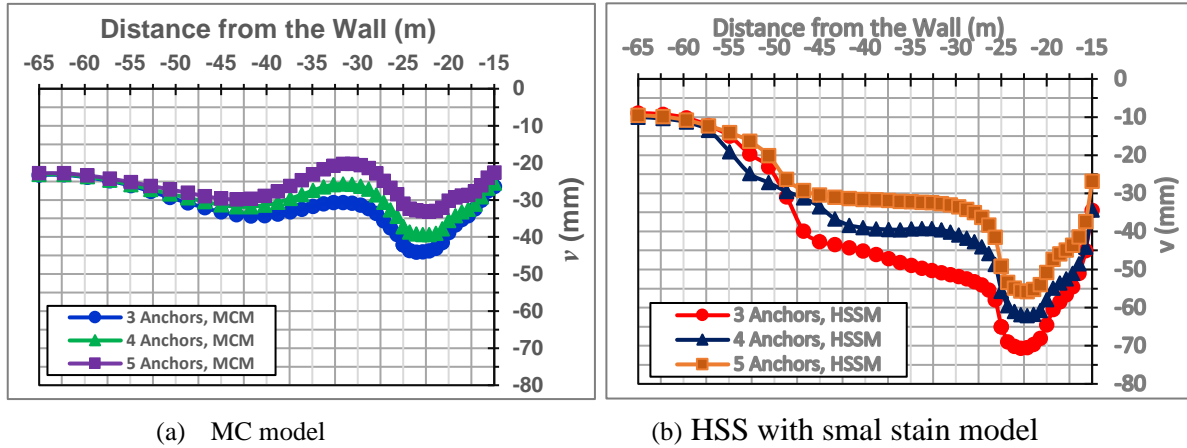


Figure 12: Variations in v with anchor numbers for $(D_b / D_{ex} = 0.7)$.

4.3 Effect of Surface Load Magnitude

An asymmetrically uniformly distributed load of (20, 30, and 40) kPa starting from 0 to 10 m from each side of the excavation edges was considered to study its effect on the maximum lateral deflection of the wall, the maximum bending moment in the wall, and the maximum ground surface settlements, and the results were then compared to the excavation without load for the particular ratio of $(D_b / D_{ex} = 0.3)$. The analysis was performed with a 0.8 m wall thickness, 4 anchors at a 15° inclination angle, and groundwater level at 16m below ground surface.

The variations of u_{xw} and M in the walls, and v with load magnitude at the end of the final excavation stage for any diaphragm wall (here the LDW is considered) due to the symmetry of the load and the model geometry are shown in Figure 13 and presented in Table 7. It is seen that as the load magnitude increases, the u_{xw} increases, whereas the M decreases compared to excavation cases under initial gravity load only (i.e., without surface load). Furthermore, based on the results at the final excavation stage as illustrated in Table 8, it was observed that with increasing load magnitude, the maximum ground surface settlement (v) increases.

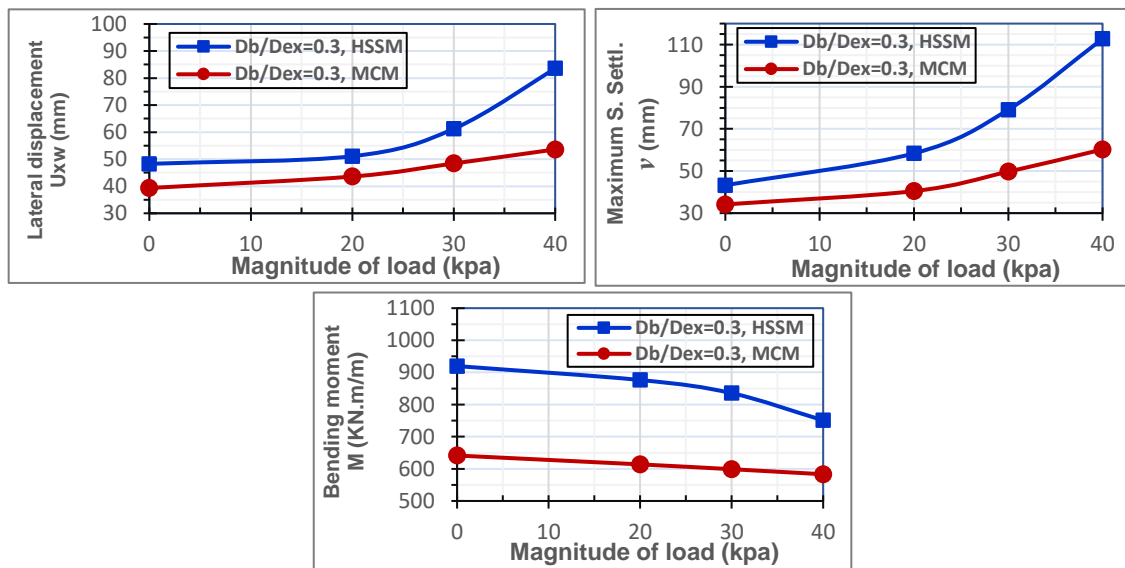


Figure 13: Variations of u_{xw} and M in the walls, and v with load magnitude

Table 7: Variations of u_{xw} and M in the LDW with load magnitude.

Magnitude of load (kPa)	Lateral displacement U_{xw} (mm)		Bending moment M (kN.m/m)			
	MCM	HSSM	MCM		HSSM	
			Max.	Min.	Max.	Min.
0	39.34	48.29	641.4	-223.6	919.7	-134.4
20	43.58	51.10	613.8	-263.4	876.4	-208.6
30	48.42	61.22	598.8	-282.2	835.5	-254.2
40	53.60	83.59	583.1	-305.0	750.9	-291.7

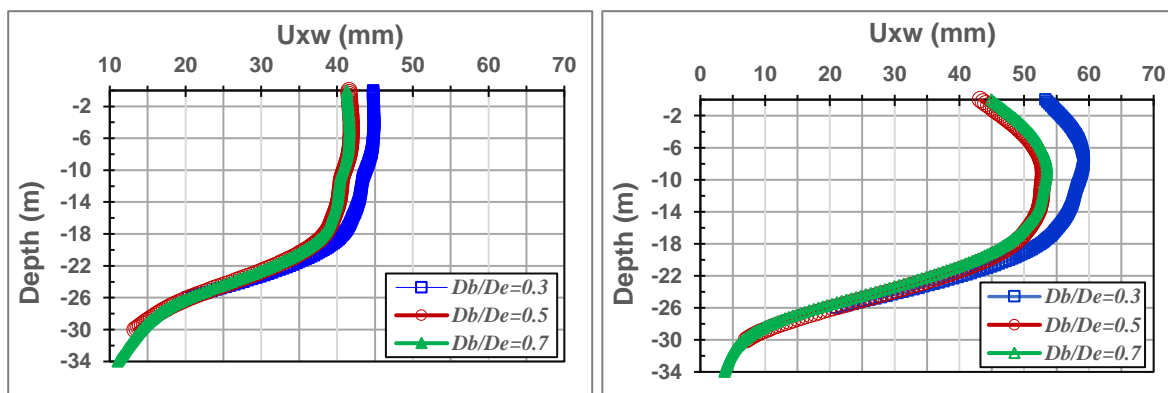
Table 8: Variations of (v) with load magnitude for $(D_b/D_{ex} = 0.3)$ –final excavation.

Magnitude of load (kPa)	Max. ground surface settlement v (mm)	
	MCM	HSSM
0	34.12	43.23
20	40.45	58.37
30	49.67	79.08
40	60.24	112.8

4.4 Effect of Embedded Depth of Diaphragm Wall

In this series, the embedded depth (D_b) was normalized to the excavation depth (D_{ex}). Three values of the non-dimensional parameter ($D_b/D_{ex} = 0.3, 0.5, \text{ and } 0.7$) were considered to study their effects on the response of the anchored diaphragm wall supporting system in terms of the maximum lateral deflection of the wall, maximum bending moment in the wall, and maximum ground surface settlements. The analysis was carried out with 4 ground anchors at $\alpha = 15^\circ$, two diaphragm walls each of $t_{wall} = 0.8 \text{ m}$, and uniformly distributed loads of $10 + 40 \text{ kPa}$ acting from 0 to 10 m from the left and right edges of the excavation.

Figure 14 depicts the variations of u_{xw} , and M across each diaphragm wall depth, as well as the ground surface settlement v behind each excavation side at the final excavation stage for different (D_b/D_{ex}) .



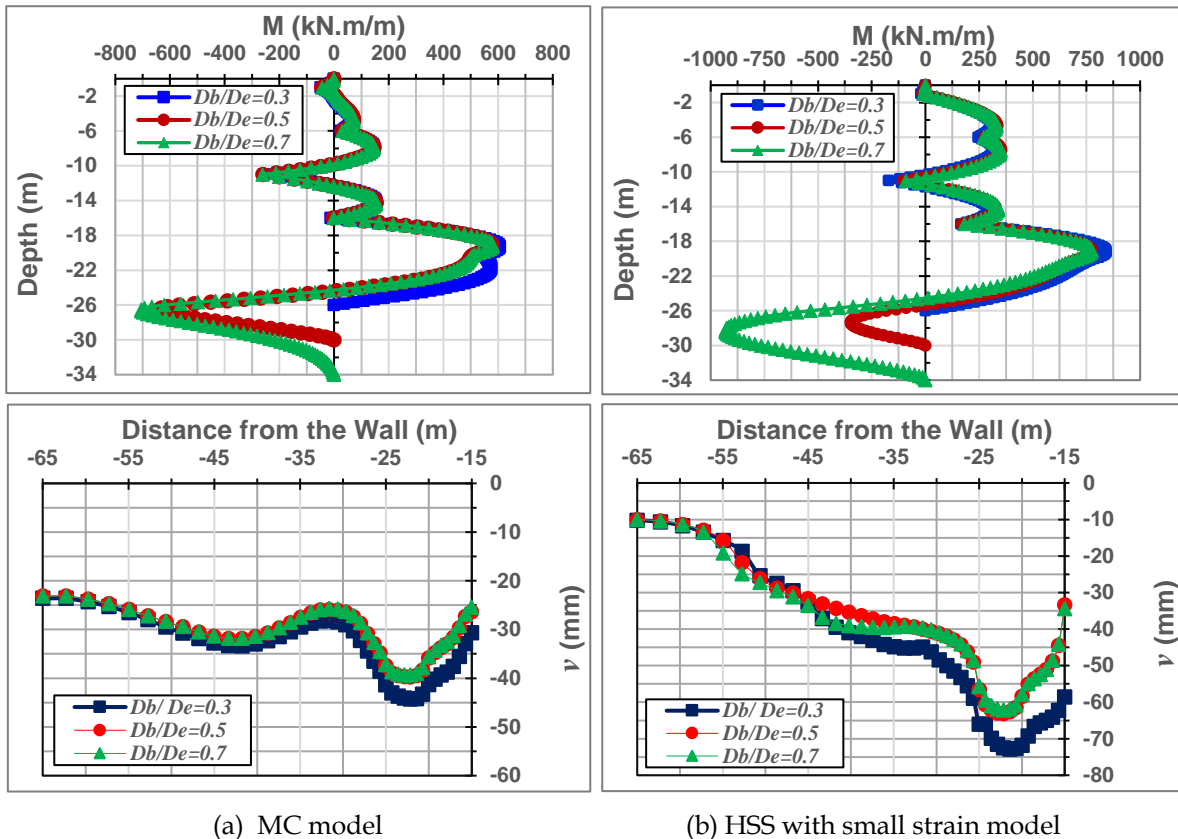


Figure 14: Variations in u_{xw} , M , v with depth at final excavation stage.

The effect of the embedded depth of the diaphragm wall on each of the u_{xw} , M and v values at the end of the final excavation stage is shown in Table 9. It is observed that when increasing D_b/D_{ex} from 0.3 to 0.5, the lateral displacement of each wall is reduced by about 6.7% and 10.5% for MC and HSsmall constitutive models, respectively. While further increasing D_b/D_{ex} to 0.7 for both models, the u_{xw} values are approximately unchanged. Similarly, when increasing D_b/D_{ex} from 0.3 to 0.5, the bending moment in each wall decreases by about 4.7% for MC and by about 8.1% for HSsmall soil modeling, and with increasing D_b/D_{ex} to 0.7 for both models, the M values are approximately no longer decreased. Furthermore, the effect of D_b on the maximum ground surface settlement variations behind each excavation side is also illustrated in Table 9. It is found that the settlement v decreases with increasing D_b/D_{ex} from 0.3 to 0.5, and when this ratio reaches 0.7, the settlement is nearly unchanged.

Therefore, the reasonable embedded depth of the diaphragm wall is 14 m (i.e., at $D_b/D_{ex} = 0.7$). Furthermore, Figure 15 demonstrates the comparison of MC and HSsmall soil models in terms of the maximum u_{xw} , and M developed in the walls, as well as the maximum ground surface settlement v during each excavation stage for the case of $D_b/D_{ex} = 0.7$. The analysis results show that the HSsmall model gives quite more accurate results than MCM when modeling such problems.

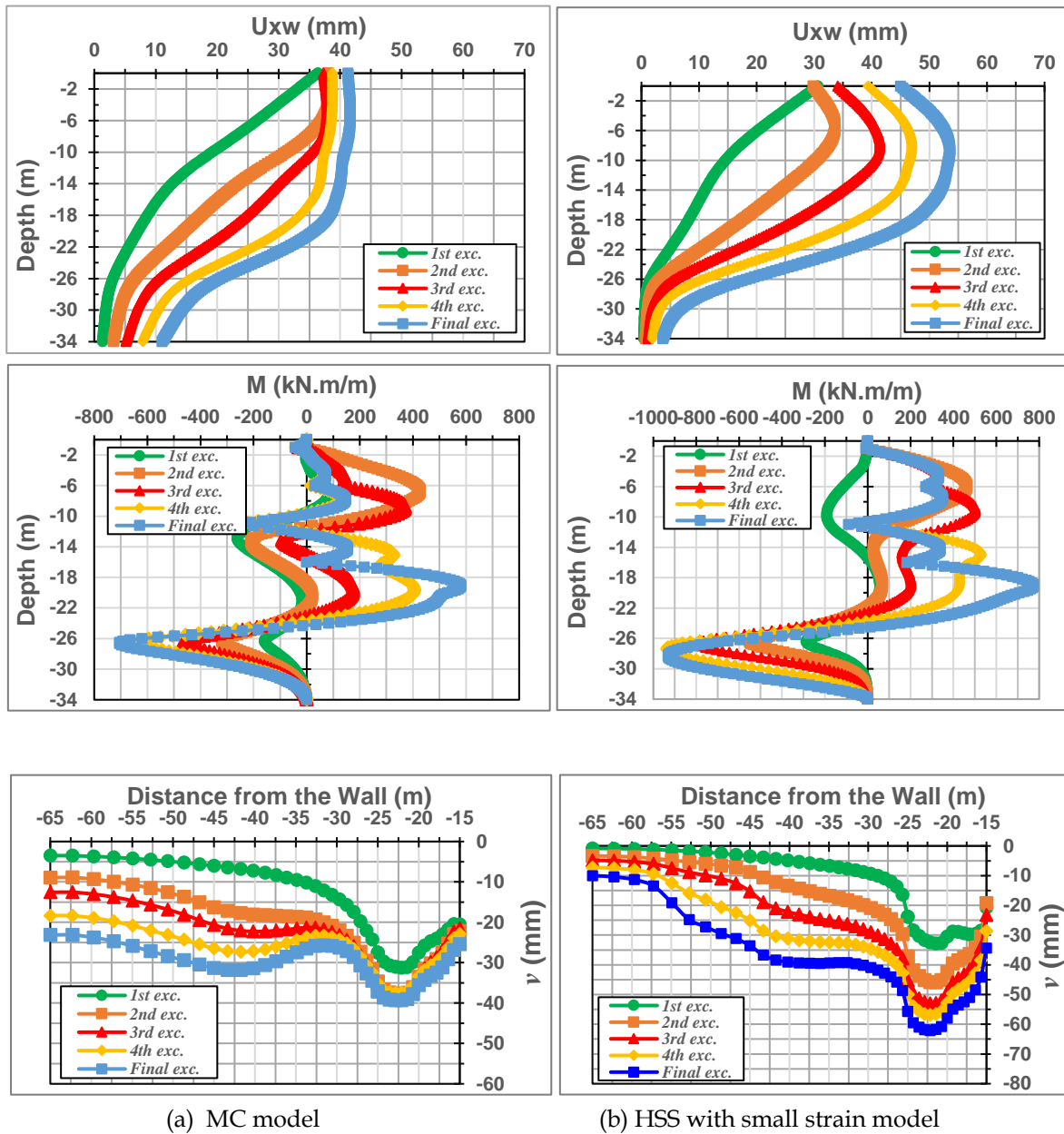


Figure 15: Variations of u_{xw} , M and v with excavation stages for $(D_b / D_{ex} = 0.7)$.

4.5 Heave at the ground-bottom of the excavation

Due to the soil excavation (unloading), the in-situ soil is subjected to a change of stress, causing a reduction in both total stress, and pore-water pressure, and as a result, the heave at the bottom of the excavation will develop gradually. In this section, the ground-bottom heave is examined at the end of the final excavation for different D_b / D_{ex} ratios and using a different number of anchors. Generally, the analysis results show that as the excavation stages progressed, the amount of heave increased. The variation of the heave at the bottom of the excavation and the safety factors at the final excavation stage with D_b / D_{ex} any number of anchors are illustrated in Figure 16.

It is seen that for any number of anchors, the heave in the case of the MC soil model is almost unchanged. The same trend is noticed even when D_b / D_{ex} or the number of anchors is increased. While in the case of HSmall, the heave decreased with increasing diaphragm wall length or anchoring number. On the other hand, for both constitutive soil models, the corresponding safety factors increased due to the stability improvement of the diaphragm walls with a

larger embedded depth. Furthermore, for both soil modeling, when the number of anchors > 4 , the decrease in heave amounts or the improvement in safety factors with increasing D_b / D_{ex} is unchanged. Therefore, the best results were obtained when the anchor number is 4 and the embedded depth of the diaphragm wall is 14 m (i.e., at $D_b / D_{ex} = 0.7$).

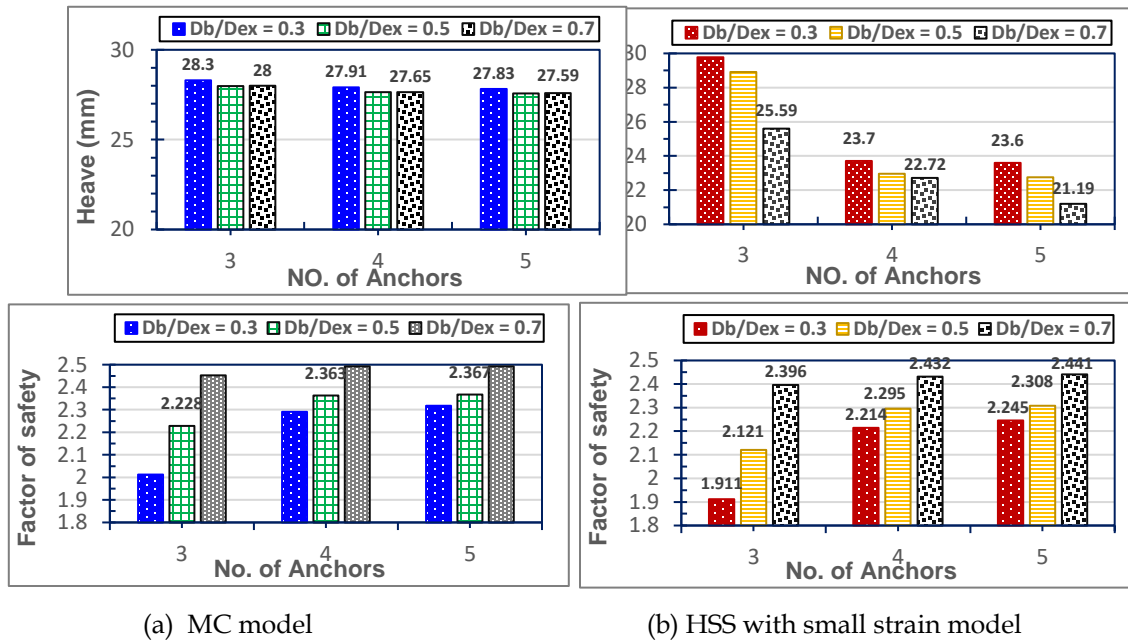


Figure 16: Variations of heave and safety factor with anchor numbers and D_b / D_{ex} .

The variations of heave amounts across the excavation width for all D_b / D_{ex} ratios and both constitutive soil models when four ground anchors were used to support each diaphragm wall on each excavation side are illustrated in Figure 17. It is seen that in all D_b / D_{ex} cases studied, the amount of heave induced at the bottom of the excavation produced by the HSsmall model was greater near the diaphragm walls than near the center of the excavation as produced by the MCM. The difference in the resulting trends obtained by the two models is referred to the capability of the HSsmall model for simulating the soil deformations during staged excavation (unloading) compared to the Mohr-Coulombs model. Also, it was found that the heave values produced by the MCM are 27.91, 27.64, and 27.65 mm for $D_b / D_{ex} = 0.3, 0.5,$ and 0.7 , respectively, which are greater than those obtained by the HSsmall model, hence their values are 23.70, 22.96, and 22.72 mm for the same D_b / D_{ex} ratios.

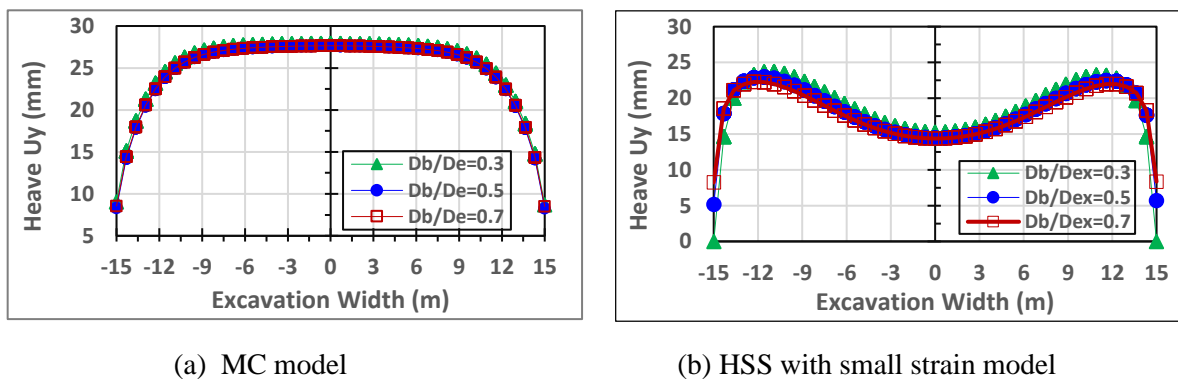


Figure 17: Variations of heave vs. D_b / D_{ex} ratios with four ground anchors.

5. Conclusions

This paper highlights the importance of using the (HSsmall) model in numerical modeling of deep excavation supported by anchored diaphragm walls using Plaxis 2D in different scenarios. The key concluding points from the analysis of the presented work are:

- The values of lateral or vertical wall displacements, wall bending moments, and the ground surface settlement on both sides of the excavation u_{xw}, M, v decrease with an increase in the angle of the ground anchor up to $\alpha = 15^\circ$. A similar trend was observed in the left and right diaphragm walls, although the surface-applied load behind each wall is different.
- As supports for the diaphragm walls on each side of the excavation, the reasonable number of ground anchors is found to be four, hence, the behavior of the supporting system is significantly improved each of u_{xw}, M , and v .
- As the load magnitude increases, each of u_{xw} and v increases, whereas the M decreases compared to excavation cases under initial gravity load only (i.e., without surface load).
- For both MC and HSsmall constitutive soil models, the reasonable embedded depth of the diaphragm wall is found to be 14 m (i.e., at $D_b / D_{ex} = 0.7$).
- Accordance to the analysis results of all studied design factors, the HSsmall model gives quite more accurate results than Mohr-Coulomb's model when modeling such problems.
- In all D_b / D_{ex} cases studied, the amount of heave induced at the bottom of the excavation produced by the HSsmall model was greater near the diaphragm walls than near the center of the excavation as produced by the MCM. As well as, the amount of heave values produced by the MCM are greater than those obtained by the HSsmall model.

6. Conflicts of interest

The authors declare that they have no conflicts of interest regarding the publication of this paper.

7. References

- [1] Abdel-Fattah, E.-S., A. A. E. Hegazy and E. M. A. G. Awaad (2018) "Analysis of the behavior of inclined anchor by varying the inclination and elevation of a tie."
- [2] Bathe, K.-J. (1996). "Finite Element Procedures Prentice-Hall." New Jersey 1037: 1.
- [3] Brinkgreve, R., L. Zampich and N. Ragi Manoj (2019). "PLAXIS Scientific Manual CONNECT Edition V20." Delft, Netherlands.
- [4] Capraru, C. and A. Chirica (2012). "Numerical modeling and constitutive soil models for deep excavations analysis." International Multidisciplinary Scientific GeoConference: SGEM 2: 215.
- [5] Chowdhury, S. S., K. Deb and A. Sengupta (2013). "Estimation of design parameters for braced excavation: a numerical study." International Journal of Geomechanics 13(3): 234-247.
- [6] El-Nahas, F. and M. Morsy (2002). Comparison of the measured and computed performance of propped diaphragm retaining wall in Egypt. Proc. of the Int. Symposium on Numerical Models in Geomechanics, Rome, Italy.
- [7] Engin, A. (2019). Finite element analysis of a deep excavation: a case study, Middle East Technical University.
- [8] Fayed, A. (2002). Numerical modeling of underground subway stations, Ph. D. Thesis, Geotechnical and Foundation Engineering, Ain Shams University
- [9] Johansson, E. and E. Sandeman (2014). Modelling of a deep excavation in soft clay a comparison of different calculation methods to in-situ measurements.
- [10] Korff, M., R. Mair, A. Van Tol and F. Kaalberg (2012). "The response of piled buildings to deep excavations." Geotechnical aspects of underground construction in soft ground. London: Taylor & Francis.
- [11] Li, L.-x., J.-d. Liu, K.-j. Li, H. Huang and X. Ji (2019). "Study of parameters selection and applicability of HSS model in a typical stratum of Jinan." Rock Soil Mech 40 (10): 4021-4029.

- [12] Likitlersuang, S., C. Surarak, D. Wanatowski, E. Oh and A. Balasubramaniam (2013). "Finite element analysis of a deep excavation: A case study from the Bangkok MRT." Soils and Foundations **53**(5): 756-773.
- [13] Mei, Y., D. Zhou, X. Wang, L. Zhao, J. Shen, S. Zhang and Y. Liu (2021). "Deformation law of the diaphragm wall during deep foundation pit construction on the lake and sea soft soil in the Yangtze River Delta." Advances in Civil Engineering **2021**.
- [14] Mitew-Czajewska, M. (2017). FEM modeling of deep excavation-parametric study, HypoplasticClay model verification. MATEC Web of Conferences, EDP Sciences.
- [15] Mitew-Czajewska, M. (2018). "Parametric study of deep excavation in clays." Bulletin of the Polish Academy of Sciences. Technical Sciences **66** (5).
- [16] Obrzud, R. F. (2010). "On the use of the Hardening Soil Small Strain model in geotechnical practice." Numerics in geotechnics and structures **16**: 1-17.
- [17] Schweiger, H. (2009). Influence of constitutive model and EC7 design approach in FEM analysis of deep excavations. ISSMGE Int. Seminar on Deep Excavations and Retaining Structures, ISSMGE Hungarian National Committee.
- [18] Schweiger, H. and H. Breymann (2006). FE-analysis of five deep excavations in lacustrine clay and comparison with in-situ measurements. Geotechnical aspects of underground construction in soft ground. Proceedings of the 5th international conference of TC 28 of the ISSMGE, the Netherlands, 15-17 June 2005.
- [19] Schweiger, H. F. (2007). "Modelling issues for numerical analysis of deep excavations." Institute for Soil Mechanics and Foundation Engineering Graz University of Technology, Austria.
- [20] Tjie-Liong, G. (2014). "Common mistakes on the application of Plaxis 2D in analyzing excavation problems." International Journal of Applied Engineering Research **9** (21): 8291-8311.
- [21] Zain, M. N., J. Ahmad, Y. Ashaari, E. Shaffie and N. Mustaffa (2011). Modeling of Lateral Movement in Soft Soil Using Hardening Soil Model. 2011 UkSim 13th International Conference on Computer Modelling and Simulation, IEEE.
- [22] Kulkarni S. R. 'Analysis of deep excavation using PLAXIS 2D'. M tech Thesis, Department of Civil Eng, COEP (2014).